Supporting Information for

Anthropogenic Modulation of Dust-Dominated Ice Nucleation in an Urban Dryland City of China

Chengqing Chen[1], Yang Wang[1*], Jiming Li[1], Lu Feng[1], Tianrong Chai[1], Zhao Ji[1], Jian Wang[2], Yuan Wang[1]

[1]College of Atmospheric Sciences and Key Laboratory for Semi-Arid Climate Change of the Ministry of Education, Lanzhou University, Lanzhou, 730000, China

[2]Nanjing Handa Environmental Technology Co., Ltd., Nanjing, 211102, China

Correspondence to: Yang Wang (wang_yang@lzu.edu.cn)

Contents

Text S1. Definition and Calculation Methods of Normalized Ice Nucleation Parameters

In this study, to systematically evaluate the ice-nucleating ability of different aerosol components, we employed multiple normalization methods to characterize ice nucleation activity (Moore et al., 2025). The activation fractions $N_{D>0.5}$ and $N_{D>1.0}$ represent the observed INPs concentration normalized to the number concentration of aerosol particles with diameters greater than 0.5 μm ($n_{0.5}$) and 1 μm ($n_{1.0}$), both constrained to particles smaller than 2.5 μm. respectively. Their corresponding equations are provided as Eq.(1) and Eq.(2). In addition, normalization parameters based on the total aerosol surface area (SA_{tot}) and volume (V_{tot}), denoted as N_s and N_v, respectively, were used. Their calculation methods are shown in Eq.(3) and Eq.(4). These two indicators reflect the nucleation potential per unit surface area and per unit volume, respectively.

$$N_{\mathrm{D>0.5}}(\mathrm{T}) = \frac{N_{\mathrm{INP}}(\mathrm{T})}{n_{0.5}} \tag{1}$$

$$N_{\mathrm{D>1.0}}(\mathrm{T}) = \frac{N_{\mathrm{INP}}(\mathrm{T})}{n_{1.0}} \tag{2}$$

$$N_{\mathrm{s}}(\mathrm{T}) = \frac{N_{\mathrm{INP}}(\mathrm{T})}{SA_{\mathrm{tot}}} \tag{3}$$

$$N_{\mathrm{v}}(\mathrm{T}) = \frac{N_{\mathrm{INP}}(\mathrm{T})}{V_{\mathrm{tot}}} \tag{4}$$

Text S2. Empirical parameterization schemes for INPs

To quantitatively describe the relationship between INP concentrations, temperature, and aerosol properties, we constructed two empirical parameterization models.

Following the exponential form of Meyers et al. (1992), a single-parameter model was established with air temperature (T, in K) as the sole predictor (Eq.(5)):

$$N_{\mathrm{IN,T_k}} = \exp[a_1 + b_1\,(273.15 - \mathrm{T_k})] \tag{5}$$

where a_1 and b_1 are regression coefficients fitted to the observed dataset. The second scheme adopts the framework of DeMott et al. (2010), which originally incorporated $n_{0.5}$ together with temperature. In this study, we modified the predictor to $n_{1.0}$, in order to better represent coarse-mode aerosols observed in Lanzhou, and re-fitted all coefficients using the measurement dataset (Eq.(6)):

$$n_{IN,T_k} = a_2(273.16 - T_k)^{b_2}(n_{1.0})(c_2(273.16 - T_k) + d_2) \quad (6)$$

where a_2, b_2, c_2, d_2 are empirical fitting parameters.

Text S3. Definition and modification of the sensitivity metric A^{-1}

A sensitivity metric $A_{dust,lab}$ to quantify the relative importance of temperature and dust abundance for immersion freezing (Villanueva et al., 2025). Based on laboratory constraints, INP concentrations were expressed as a function of the logarithm of dust aerosol optical depth (LD) and temperature (T):

$$INP_{dust}(T,LD) = C_1 \cdot LD \cdot \exp(-A_{dust,lab}\, T) \quad (7)$$

where $A_{dust,lab}$ (K^{-1}) is the slope parameter governing temperature sensitivity. By definition, as shown in Eq.(6).

$$A_{dust,lab} = \frac{\left(\frac{\partial INP}{\partial T}\right)}{\left(\frac{\partial INP}{\partial LD}\right)} \quad (8)$$

In our observational framework, we adapt this metric to surface measurements by replacing dust aerosol optical depth (DAOD) with Fine mineral dust (FMD) mass concentration as a robust proxy for mineral dust. In addition, secondary inorganic aerosol (SNA) is included as a marker of secondary aerosols, allowing us to assess how pollution modulates the dust-temperature sensitivity balance. Specifically, we employ the following log-linear regression model:

$$\ln(INP) = b_0 + b_1 \ln(FMD) + b_2\,(-T) + b_3 \ln(SNA) + b_4\,[\ln(FMD)\ln(SNA)] + \varepsilon \quad (9)$$

where b_1 represents the main effect of FMD, b_2 the temperature sensitivity, b_3 the main effect of SNA, and b_4 the FMD–SNA interaction term. The term ε denotes the residual error.

From this regression model, the dust sensitivity conditional on SNA is given by:

$$\frac{\partial \ln(INP)}{\partial \ln(FMD)} = b_1 + b_4\, z, \quad z = \ln(SNA) \quad (10)$$

while the temperature sensitivity is:

$$\frac{\partial \ln(INP)}{\partial(-T)} = b_2 \quad (11)$$

Accordingly, we define the observational A and A^{-1} as:

$$\mathrm{A(z)} = \frac{b_2}{b_1 + b_4\, z} \text{ and } \mathrm{A^{-1}(z)} = \frac{b_1 + b_4\, z}{b_2} \quad (12)$$

where A (K^{-1}) denotes the number of "e-fold dust increases" equivalent to 1 K cooling, and A^{-1} (K^{-1}) denotes the effective cooling equivalent to one e-fold (i.e., based on the natural exponential e) dust increase.

Text S4. Calculation Equation for ice nucleation activity evaluation index

To evaluate the fitting accuracy of INP parameterization, this study used three statistical metrics: coefficient of determination (R^2), root-mean-square error (RMSE), and fraction of predictions within a factor of 5 (FAC_5). The formulas are provided in Eq.(13–15). All metrics are computed in the natural log space (ln) to mitigate the influence of data with different orders of magnitude on the statistical results.

$$R^2 = 1 - \frac{\sum_{i=1}^{n}\left[\ln\left(N_{\mathrm{obs},i}\right) - \ln\left(N_{\mathrm{fit},i}\right)\right]^2}{\sum_{i=1}^{n}\left[\ln\left(N_{\mathrm{obs},i}\right) - \overline{\ln(N_{\mathrm{obs}})}\right]^2} \quad (13)$$

$$\mathrm{RMSE} = \sqrt{\frac{1}{n}\sum_{i=1}^{n}\left[\ln\left(N_{\mathrm{obs},i}\right) - \ln\left(N_{\mathrm{fit},i}\right)\right]^2} \quad (14)$$

$$\mathrm{FAC_5} = \frac{1}{n}\sum_{i=1}^{n}\left[\left|\ln\left(N_{\mathrm{fit},i}\right) - \ln\left(N_{\mathrm{obs},i}\right)\right| \le \ln(5)\right] \times 100\% \quad (15)$$

Here, $N_{\mathrm{obs,i}}$ and $N_{\mathrm{fit,i}}$ represent the observed and predicted INP concentrations, respectively. The variable n is the sample size.

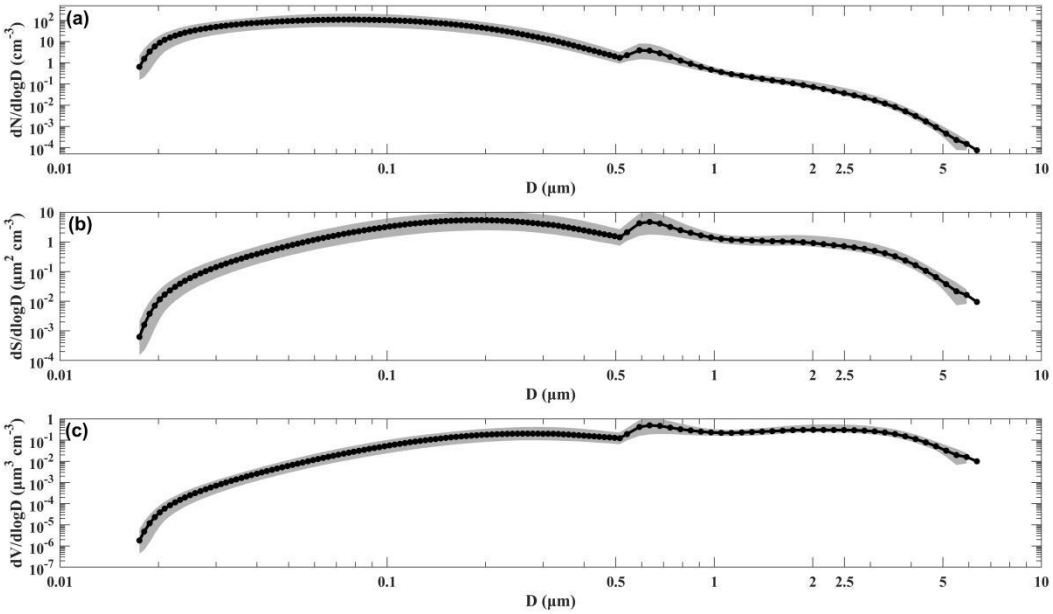

Fig. S1. Aerosol Size Distribution Characteristics. (a) Particle Number Density Distribution. (b) Surface Area Density Distribution. (c) Volume Density Distribution. The black solid circles represent the median for all time periods in each particle size range, and the grey shading denotes the range between the 25th and 75th percentiles.

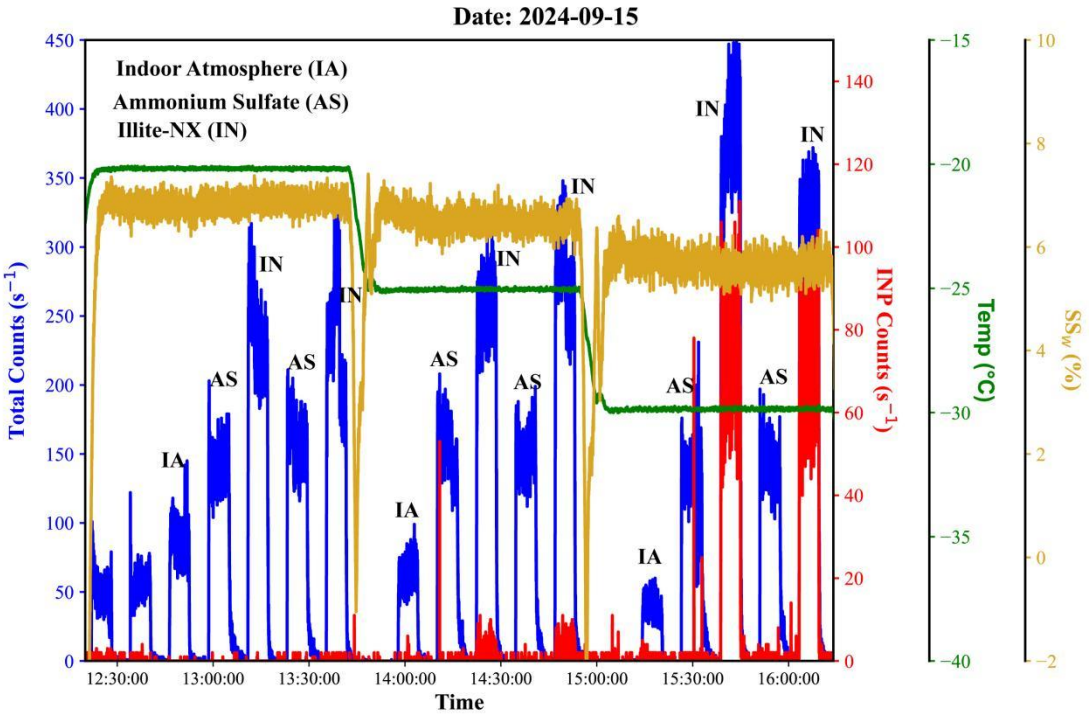

Fig. S2. Aerosol ice nucleation activity tests performed at different temperatures under identical supersaturation conditions. Indoor atmospheric samples, ammonium sulfate, and illite-NX were tested separately for their ice nucleation activity. The figure presents time series at one-second resolution for total particle count, INPs count, temperature, and supersaturation relative to water (SS_w).

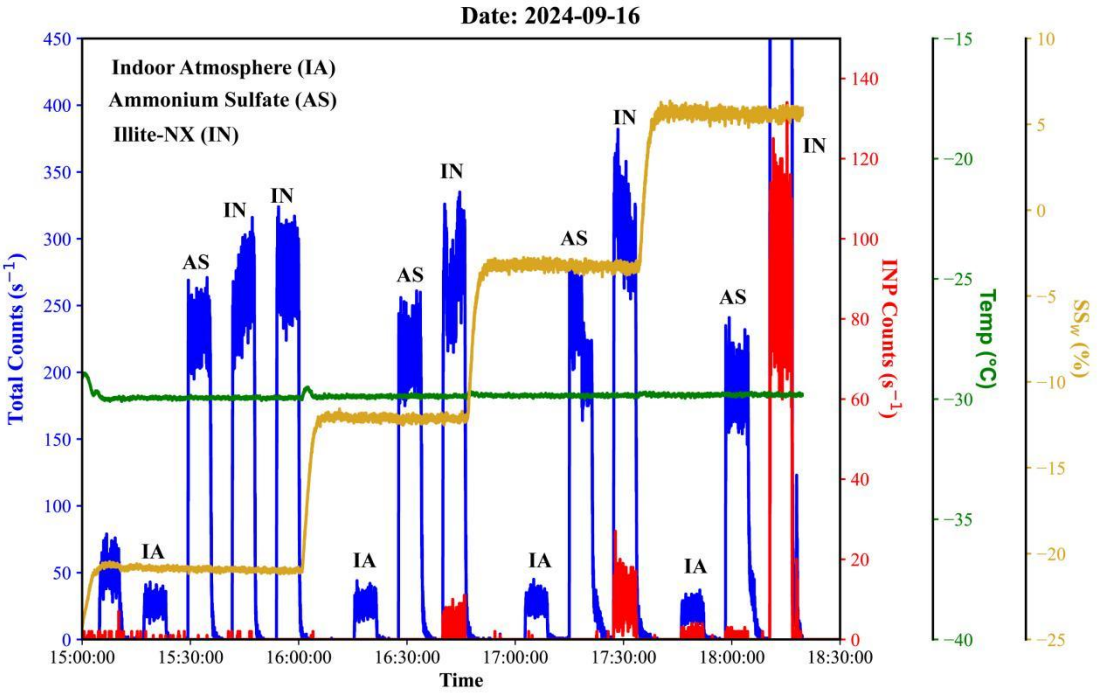

Fig. S3. Ice nucleation activity test of aerosol particles under different supersaturation conditions at a constant temperature. Indoor atmospheric samples, ammonium sulfate, and illite-NX were tested separately for their ice nucleation activity. The figure presents time series at one-second resolution for total particle count, INPs count, temperature, and supersaturation relative to water (SS_w) .

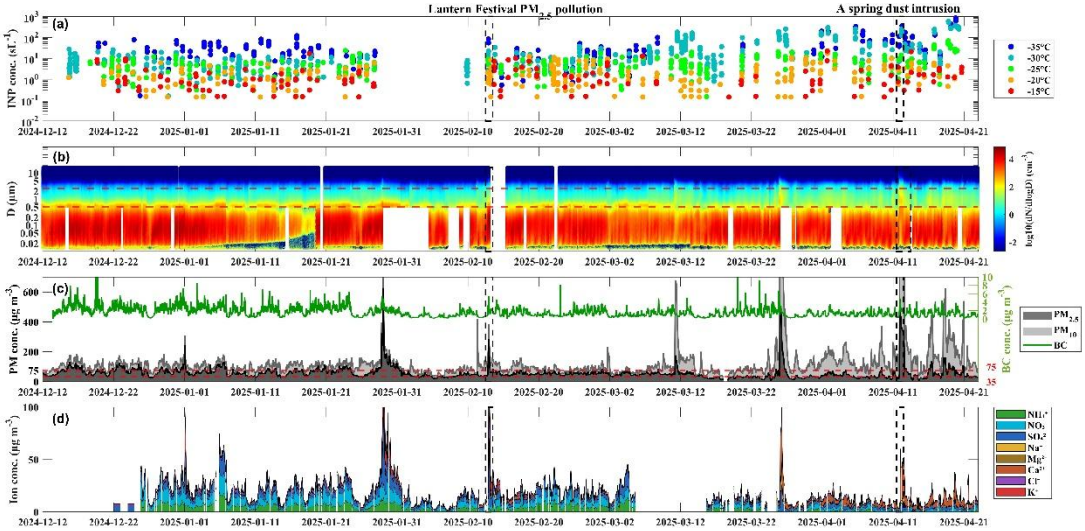

Fig. S4. Time series of INPs and aerosol characteristics. (a) INP concentrations at five activation temperatures. (b) Aerosol particle size distribution. The red dashed lines indicate particle sizes of 0.5 μm and 2.5 μm. Data gaps are shown as blank areas. (c) Aerosol mass concentration and BC mass concentration. The red dashed lines indicate reference values of 35 (μg m^{-3}) and (75 μg m^{-3}). (d) Water-soluble ion mass concentration.

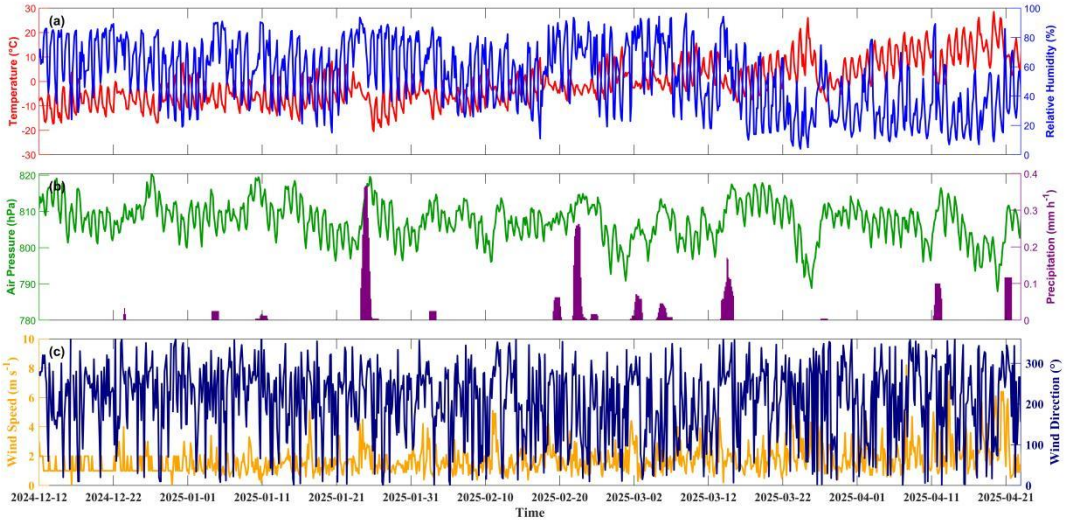

Fig. S5. Time series of key meteorological variables at the Yuzhong meteorological station. (a) Temperature and relative humidity. (b) Air pressure and precipitation. (c) Wind speed and direction. The station is located approximately 30 km from the sampling site. Data source: NOAA National Centers for Environmental Information, Global Surface Hourly Data for Station 529830-99999 (Yuzhong), China, 2010–2020; accessed June 1, 2025.

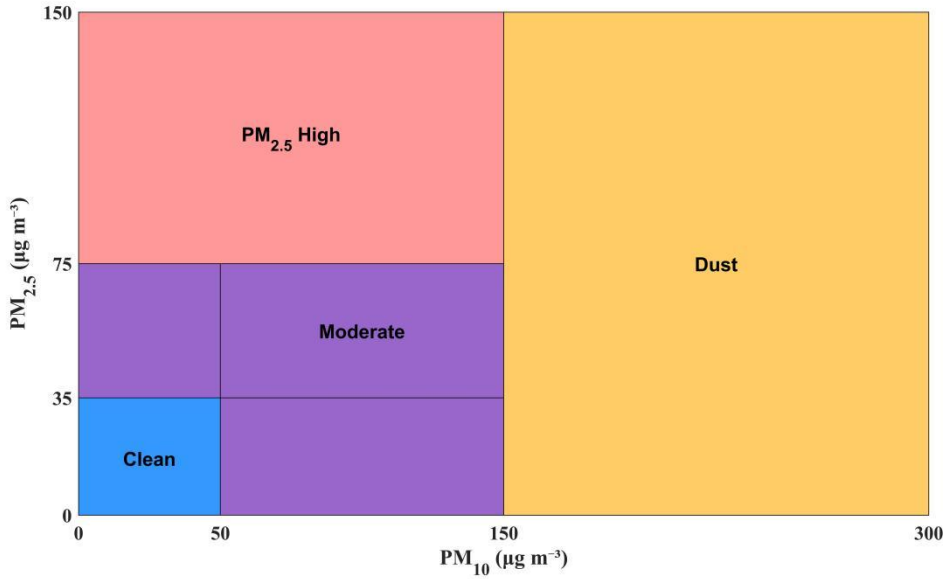

Fig. S6. Aerosol type classification based on PM_{10} and $PM_{2.5}$ concentrations. Four categories are defined using threshold values of $PM_{2.5}$ (35, 75 μg m^{-3}) and PM_{10} (50, 150 μg m^{-3}), following the Chinese National Ambient Air Quality Standards (GB3095-2012).

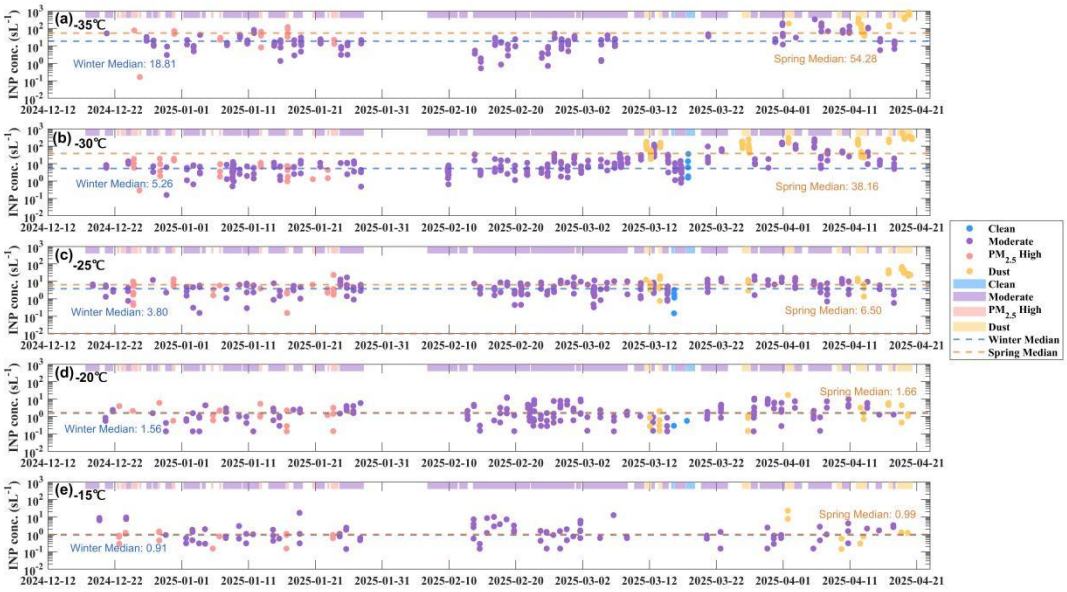

Fig. S7. Time series of INP concentrations at different temperature layers. The shaded areas in distinct colors represent the temporal distribution of different aerosol types, with the INP concentration for each aerosol type indicated by scattered points of corresponding colors. The dotted line indicates the median INP concentration for all aerosol types in winter and spring, with the values shown in the corresponding colors.

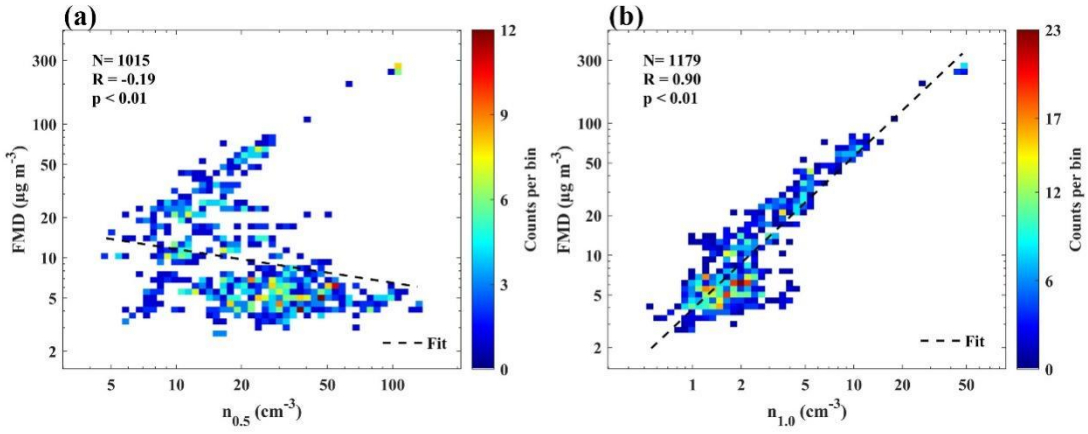

Fig. S8. Relationships between FMD and aerosol number concentrations. Two-dimensional histograms of $n_{0.5}$ and $n_{1.0}$ versus PMD, respectively. Data from five temperatures and four aerosol event types are combined. The X and Y axes are binned into 50 intervals in the natural log space, and the color shading indicates the number of samples in each bin. *N* denotes the total number of data points. *R* and *p* are the Pearson correlation coefficient and the corresponding significance level.

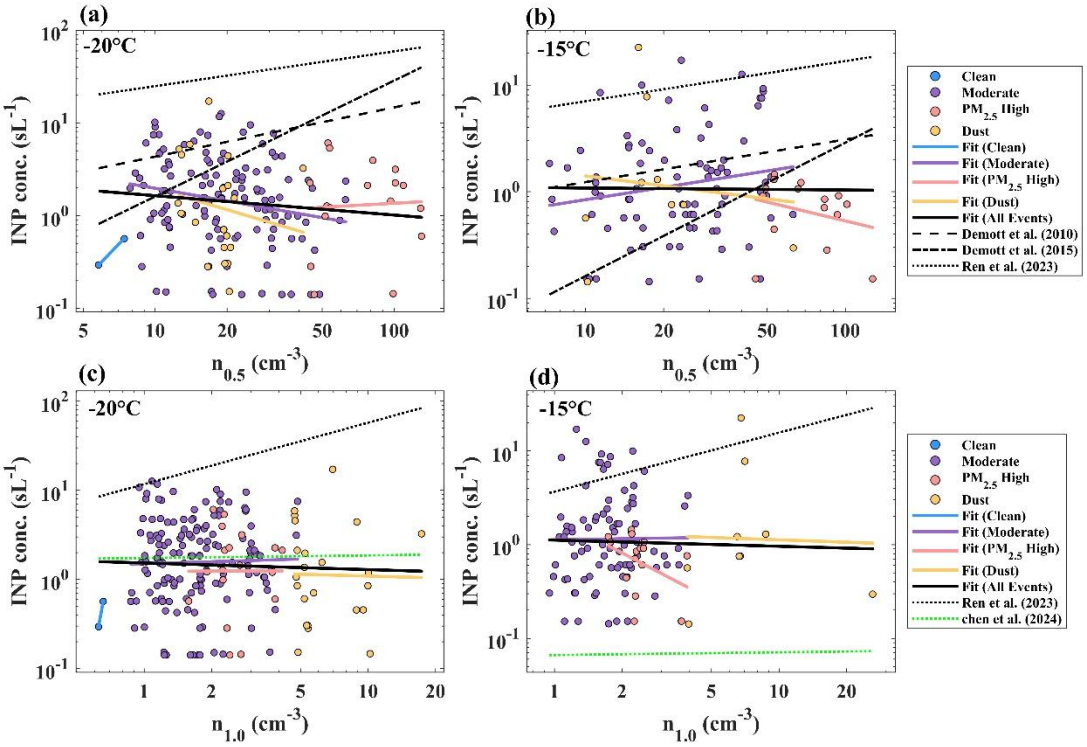

118

119 **Fig. S9. Relationships between INP concentration and aerosol number concentrations.** (a–b) show the
120 relationships between INP concentration and $n_{0.5}$, while (c–d) depict the relationships with $n_{1.0}$. The R and p values
121 represent the Pearson correlation coefficient and its significance, and only results with $p < 0.01$ are shown. The black
122 solid line shows the fit for all samples, and the black dashed line indicates the prediction from existing
123 parameterization schemes.

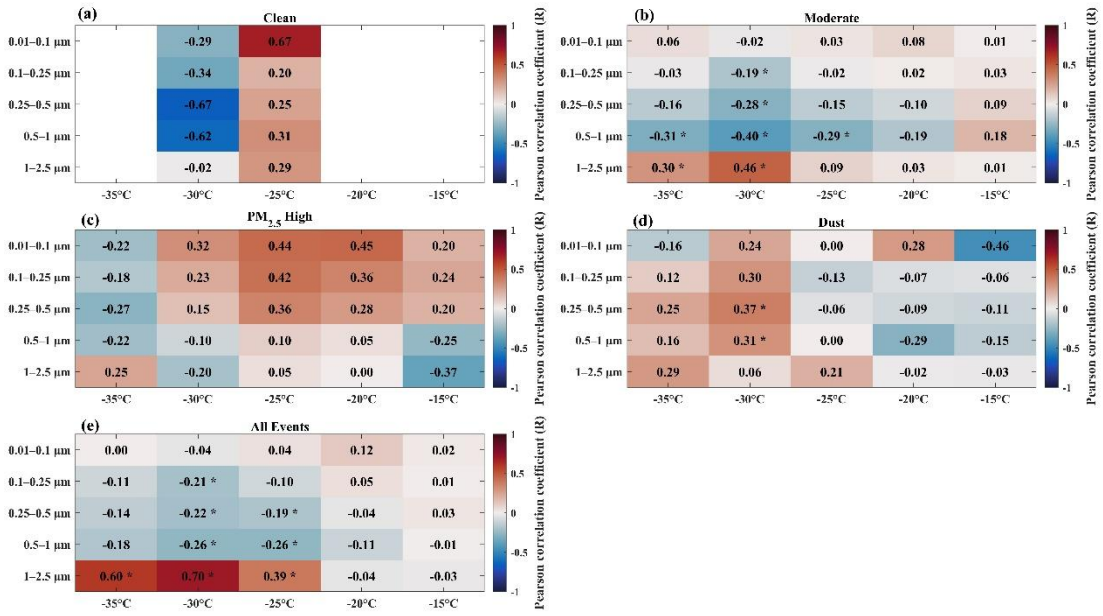

124

125 **Fig. S10. Pearson correlations between INP concentrations and aerosol particle number concentrations across**
126 **different event types.** The R represent the Pearson correlation coefficient, calculated in the natural log space.
127 Statistically significant correlations ($p < 0.01$) are marked with asterisks.

Table S1. Fitting results of single-parameter INPs models under different pollution event types

Event	a_1	b_1	R^2	RMSE	FAC_5
All Event	-3.0599	0.1875	0.39	1.40	76.33%
Clean	-6.2371	0.2597	0.44	1.06	84.62%
Moderate	-2.3477	0.1492	0.41	1.11	84.98%
PM2.5 High	-3.2722	0.1746	0.49	1.15	86.54%
Dust	-6.0673	0.3531	0.70	1.11	89.20%

Table S2. Fitting results of two-parameter models for INPs concentration prediction in Lanzhou

a_2	b_2	c_2	d_2	R^2	RMSE	FAC_5
0.0007	2.6168	0.0934	-1.6206	0. 59	1.15	82.78%

Chen, J., Wu, Z., Gong, X., Qiu, Y., Chen, S., Zeng, L., and Hu, M.: Anthropogenic dust as a significant source of ice-nucleating particles in the urban environment, Earth's Future, 12, e2023EF003738, doi:10.1029/2023EF003738, 2024.

DeMott, P. J., Prenni, A. J., Liu, X., Kreidenweis, S. M., Petters, M. D., Twohy, C. H., Richardson, M. S., Eidhammer, T., and Rogers, D. C.: Predicting global atmospheric ice nuclei distributions and their impacts on climate, Proc. Natl. Acad. Sci. U.S.A., 107, 11217–11222, doi:10.1073/pnas.0910818107, 2010.

DeMott, P. J., Prenni, A. J., McMeeking, G. R., Sullivan, R. C., Petters, M. D., Tobo, Y., Niemand, M., Möhler, O., Snider, J. R., Wang, Z., and Kreidenweis, S. M.: Integrating laboratory and field data to quantify the immersion freezing ice nucleation activity of mineral dust particles, Atmos. Chem. Phys., 15, 393–409, doi:10.5194/acp-15-393-2015, 2015.

Meyers, M. P., DeMott, P. J., and Cotton, W. R.: New primary ice nucleation parameterizations in an explicit cloud model, J. Appl. Meteorol., 31, 708–721, doi:10.1175/1520-0450(1992)031<0708:NPINPI>2.0.CO;2, 1992.

Moore, K. A., Hill, T. C. J., Madawala, C. K., Leibensperger III, R. J., Greeney, S., Cappa, C. D., Stokes, M. D., Deane, G. B., Lee, C., Tivanski, A. V., Prather, K. A., and DeMott, P. J.: Wind-driven emission of marine ice-nucleating particles in the Scripps Ocean-Atmosphere Research Simulator (SOARS), Atmos. Chem. Phys., 25, 3131–3159, https://doi.org/10.5194/acp-25-3131-2025, 2025.

Ren, Y. Z., Bi, K., Fu, S. Z., Tian, P., Huang, M. Y., Zhu, R. H., and Xue, H. W.: The relationship of aerosol properties and ice-nucleating particle concentrations in Beijing, J. Geophys. Res. Atmos., 128, e2022JD037383, doi:10.1029/2022JD037383, 2023.

Villanueva, D., Stengel, M., Hoose, C., Bruno, O., Jeggle, K., Ansmann, A., and Lohmann, U.: Dust-driven droplet freezing explains cloud-top phase in the Northern Extratropics, Science, 389, 521–525, doi:10.1126/science.adt5354, 2025.